# We are IntechOpen, the world's leading publisher of Open Access books Built by scientists, for scientists

**6,900**
Open access books available

**186,000**
International authors and editors

**200M**
Downloads

**154**
Countries delivered to

Our authors are among the

**TOP 1%**
most cited scientists

**12.2%**
Contributors from top 500 universities

CLARIVATE ANALYTICS
**BOOK CITATION INDEX**
INDEXED

**WEB OF SCIENCE**™

Selection of our books indexed in the Book Citation Index
in Web of Science™ Core Collection (BKCI)

## Interested in publishing with us?
Contact book.department@intechopen.com

Numbers displayed above are based on latest data collected.
For more information visit www.intechopen.com

# Intercalation of Poly(bis-(methoxyethoxyethoxy)phosphazene) into Lithium Hectorite

Iskandar Saada, Rabin Bissessur,
Douglas C. Dahn and Matthieu Hughes

## Abstract

Poly(bis-(methoxyethoxyethoxy)phosphazene) (MEEP) intercalated into lithium hectorite was investigated for its potential application as a solid polymer electrolyte in lithium-ion polymer batteries. Varying amounts of MEEP were intercalated into lithium hectorite, and the physical properties of the nanocomposites were monitored using powder X-ray diffraction, thermogravimetric analysis, differential scanning calorimetry, and attenuated total reflectance spectroscopy. Alternating current (AC) impedance spectroscopy was used to determine the ionic conductivity of the nanocomposites when complexed with lithium triflate salt.

**Keywords:** lithium hectorite, poly(bis-(methoxyethoxyethoxy)phosphazene), nanocomposites, solid polymer electrolytes

## 1. Introduction

The electrolyte in a lithium-ion battery is the medium through which lithium ions flow between anode and cathode. It is electrically insulating, and thus prohibits the passage of electrons. Much work has been done to develop solid-state electrolyte materials such as solid polymer electrolytes (SPEs) which have the advantage of enhanced safety compared to conventional liquid organic electrolytes. Some of the most recent research on electrolyte materials has focused on utilizing polymers such as poly(ethylene oxide) (PEO) [1] and polyphosphazenes [2, 3]. Current research on polyphosphazenes focuses on exploiting their fire-resistant properties [4], ionic conductivity [5], and as phosphazene-based dye-sensitized

solar cells [6]. Polyphosphazenes are amorphous polymers with low glass transition temperatures ($T_g$), which dictates their polymer-chain flexibility and aids in lithium-ion mobility [7].

Since the first report on poly(bis-(methoxyethoxyethoxy)phosphazene) (MEEP), **Figure 1**, an array of phosphazene-based polymers have been synthesized with diverse alkyl ether and alkoxy side groups, ultimately yielding ionically conductive polymers that are flexible. When polyphosphazenes such as MEEP are complexed with lithium salts (e.g., lithium triflate), they have been shown to possess enhanced ionic conductivity compared to PEO-based SPEs [8, 9]. Previous studies have reported that $(MEEP)_4LiCF_3SO_3$ yields ionic conductivity in the range of $2 \times 10^{-5}$ to $1 \times 10^{-4}$ S/cm at ambient temperatures [10, 11]. However, the dimensional stability of MEEP is low, so it leaks out of cells at ambient temperatures. Researchers have attempted to enhance the dimensional stability of polyphosphazenes by investigating polymer blends with PEO [12], inducing cross-linking via $^{60}$Co-gamma irradiation [8] and preparing of polyphosphazene-silicate networks [13]. One other promising approach is the intercalation of polyphosphazenes into layered structures, which act as hosts for the polymers. Due to the weak electrostatic interactions holding the layers of two-dimensional structures, the layers may be exfoliated allowing for the intercalation of ionically conductive polymers. This yields nanocomposite materials with ionically conductive properties, along with enhanced mechanical and thermal durability provided by the layered structure. Intercalation of MEEP into two-dimensional layered structures has been investigated using layered structures such as graphite oxide [10], molybdenum disulfide [14], sodium montmorillonite [15], and sodium hectorite [16], and has typically yielded ionically conductive nanocomposite materials with enhanced physical properties. In this chapter, we report on the intercalation of various amounts of MEEP into lithium hectorite.
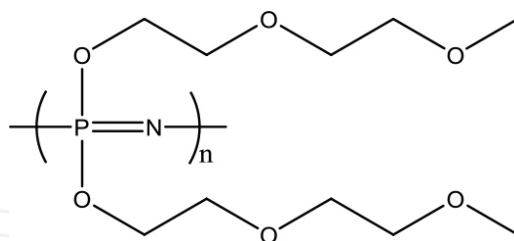


**Figure 1.** Structure of MEEP.

Hectorite belongs to the family of smectite clays, and has a 2:1 structural arrangement composed of two tetrahedral silicate layers ($T_d$) encompassing an octahedral layer ($O_h$), as shown in **Figure 2** [17]. Their industrial applications range from pharmaceutical drug additives [18] to automobile parts [19], and potentially as SPEs in batteries [20, 21]. Hectorite has negatively charged layers, which are compensated with cations such as $Na^+$ and $Li^+$ to balance the overall charge. Hectorite is an appealing layered structure for the intercalation of MEEP due to its high thermal stability, high surface area, exfoliating/restacking capability, and high cation exchange capacity [22]. In this chapter, we exploit the cation exchange capability of hectorite by driving out the naturally lying sodium ions with lithium ions, and working with

the lithiated form of hectorite [23]. The intercalation of varying stoichiometric molar ratios of MEEP was conducted with the lithiated form of hectorite.

$T_d$-$SiO_4$

$O_h$-Li, Al, Mg

$T_d$-$SiO_4$

Exchangeable cations ($Li^+$, $Na^+$) $nH_2O$
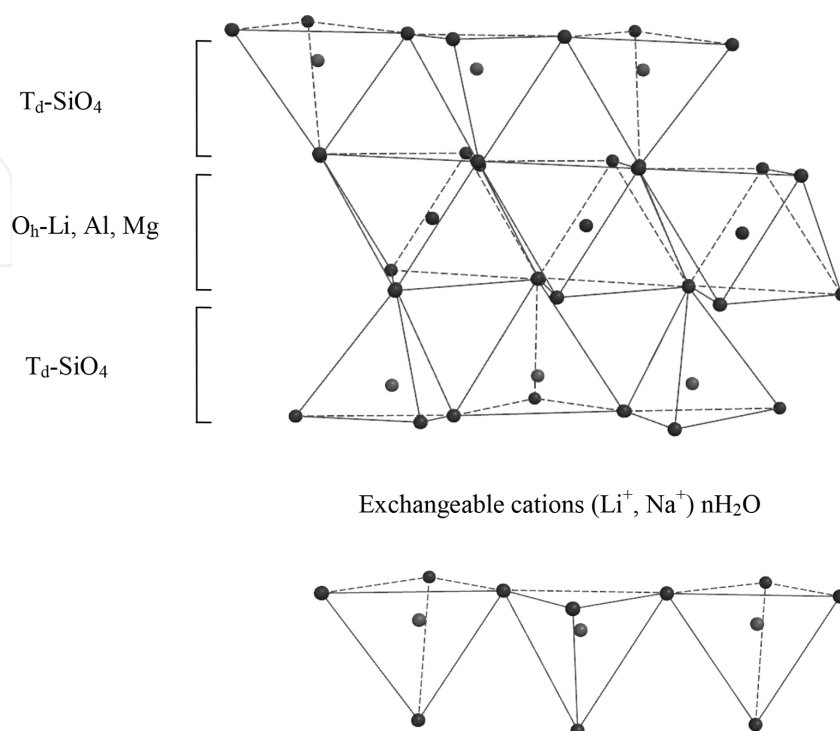
**Figure 2.** Structure of hectorite.

The aim of this chapter is to present the effects that varying polymeric molar ratios to Li-hectorite have on the physical properties of the synthesized nanocomposites, and to investigate the ionic conductivity of the salt-complexed nanocomposites. The synthesized nanocomposites were characterized using thermogravimetric analysis (TGA), differential scanning calorimetry (DSC), powder X-ray diffraction (XRD), and attenuated total reflectance (ATR). The ionic resistance of the materials was determined using AC impedance spectroscopy.

## 2. Experimental

### 2.1. Purification and lithiation of hectorite

Sodium hectorite (SHCa-1) was purchased from Source Clays Repository. Since the fine powder has calcium carbonate and other impurities, a purification process was performed as outlined in the literature [16]. When the purification process was complete, a cation exchange was done in order to replace the sodium ions with lithium ions [23]. This process was carried out twice to ensure maximum substitution of lithium ions. Elemental analysis was used to monitor the sodium- and lithium-ion content at Guelph Chemical Laboratories Ltd. Ontario, Canada. The data indicated an increase in lithium-ion proportion from $Li_{0.5}$ $Na_{0.8}$ $Si_1$ (sodium hectorite) to $Li_3$ $Na_{0.4}$ $Si_1$ (lithium hectorite).

### 2.2. Synthesis of MEEP and MEEP-salt complex

The synthesis of MEEP was performed as described in the literature [24]. $(MEEP)_4 LiCF_3SO_3$ has been found to exhibit high ionic conductivity compared to other polymer:salt ratios [13, 25], so this polymer:salt ratio was used in this work. The synthesized polymer was stored in a vacuum desiccator, and salt-polymer complexes were used as soon as they were prepared in order to minimize exposure to humidity. Hereafter, the pure (uncomplexed) polymer will be referred to as MEEP, while the salt-complexed polymer will be referred to as Li-MEEP.

### 2.3. Preparation of nanocomposites

A general procedure was employed for the intercalation of MEEP into Li-hectorite. Li-hectorite (0.10 g, $2.6 \times 10^{-4}$ mol) was suspended in deionized water and left to stir until fully suspended in water (typically 30 min). The polymer with molar ratio of 0.5, 1, 2, or 4 to Li-hectorite was dissolved in 5 mL of deionized water. A pipette was used to transfer the polymer solution to the Li-hectorite suspension at a rate of one drop per second. The progress of the reactions was monitored via XRD. The products were then isolated via freeze drying, and stored in a vacuum desiccator.

### 2.4. Materials characterization

Powder X-ray diffraction was conducted on a Bruker AXS D8 Advance diffractometer. The instrument is equipped with a graphite monochromator, variable divergence slit, variable antiscatter slit, and a scintillation detector. Cu (k$\alpha$) radiation ($\lambda = 1.542$ Å) was utilized and the data were collected at room temperature on glass substrates.

Thermogravimetric analysis (TGA) was performed on a TA Q500 using a heating rate of 10°C/min, with the use of platinum pans under dry-compressed air. Samples were freeze dried prior to TGA analysis in order to minimize their moisture content.

Differential scanning calorimetry (DSC) was performed on a TA Q100 using heat/cool/heat cycles. Samples were crimped in aluminum pans, and ran under nitrogen flow at a rate of 50 mL/min.

Attenuated total reflectance spectroscopy (ATR) data were collected using a Bruker Alpha A-T (resolution 0.9, 128 scans).

AC impedance spectroscopy (IS) was conducted to determine the ionic conductivity of the salt-complexed materials [26]. The samples were tested using rectangular glass substrates with two rectangular stainless steel electrodes on the opposite ends of the substrates. For the intercalated nanocomposites, samples were cast onto the substrates, between the electrodes, after 3 days of reaction time in order to ensure complete intercalation. Typical samples had a width of about 9 mm, were 20–90-μm thick, and had a length between the electrodes in the direction of current of about 6 mm. In most cases, the films were not uniform in thickness, and this was the main source of uncertainty in the ionic conductivity values that were obtained. The frequency range used was 10 kHz to 0.01 Hz. In order to remove moisture, the samples were placed under vacuum for at least 24 h at room temperature prior to the data collection. The temperature of

the samples was controlled using a Cryodyne 350CP refrigerator and a Lakeshore 321 temperature controller. The data collection was performed using a Solartron 1250 frequency response analyzer and a home-built accessory circuit for high-impedance samples. The conductivity was then determined by fitting the IS data to an equivalent circuit model using LEVMW [27].

# 3. Results and discussion

## 3.1. MEEP/Lithium hectorite

### 3.1.1. Powder X-ray diffraction

Powder X-ray diffraction was used to monitor the intercalation process and the effect of the molar ratio of MEEP to Li-hectorite on the polymer loading in the layered structure.
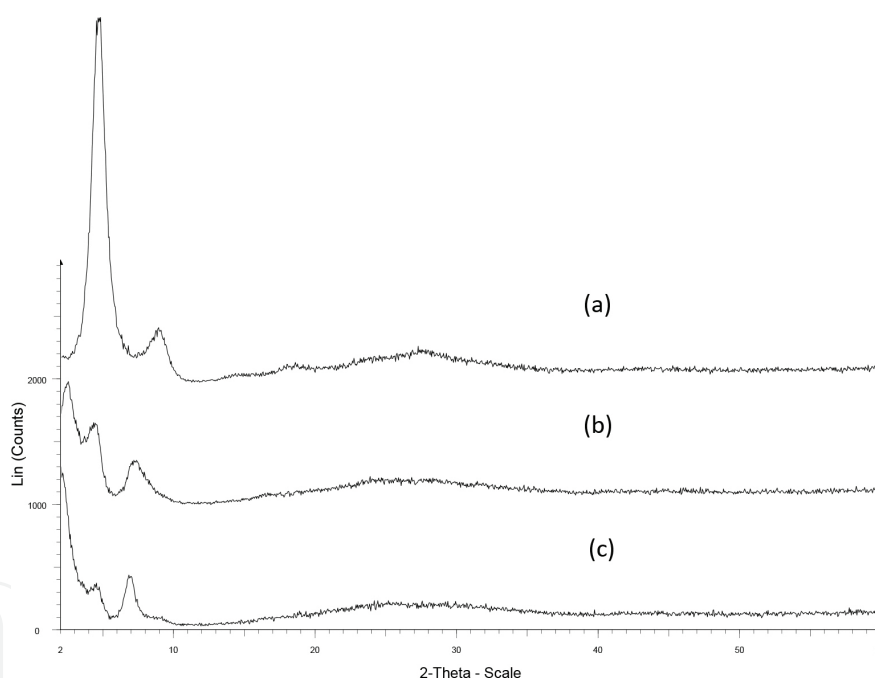


**Figure 3.** XRD data for (a) MEEP:Li-hectorite (0.5:1), (b) MEEP:Li-hectorite (2:1), and (c) MEEP:Li-hectorite (4:1).

The diffractograms for MEEP:Li-hectorite (0.5:1), MEEP:Li-hectorite (2:1), and MEEP:Li-hectorite (4:1) nanocomposites are displayed in **Figure 3** to illustrate the enhancement in basal spacing (d-spacing) of the layered host upon the intercalation of MEEP. The net interlayer expansion is obtained by subtracting the basal spacing of dry Li-hectorite heated to 650°C (d-spacing = 9.5 Å) from the basal spacing of the synthesized nanocomposite. For example, MEEP:Li-hectorite (0.5:1) nanocomposite has a basal spacing of 18.9 Å, which corresponds to an interlayer expansion of 9.40 Å. The XRD data for all the nanocomposites are summarized in **Table 1**.

| Material | Basal spacing (Å) | Net expansion (Å) | Average crystallite size (Å) |
|---|---|---|---|
| MEEP:Li-hectorite (0.5:1) | 18.9 | 9.40 | 73 |
| MEEP:Li-hectorite (1:1) | 21.7 | 12.2 | 74 |
| MEEP:Li-hectorite (2:1) | 36.4 | 26.9 | 126 |
| MEEP:Li-hectorite (4:1) | 41.5 | 32.0 | 135 |
| Na-hectorite | 10.0 | – | 140 |
| Dry Li- hectorite | 9.50 | – | 182 |

**Table 1.** Summary XRD data of hectorites and MEEP:Li-hectorite nanocomposites.

The synthesized nanocomposites are crystalline as indicated by XRD, and a significant increase in basal spacing is observed as the ratio of MEEP to Li-hectorite is increased. From the XRD diffractograms of the nanocomposites, the average crystallite size was determined using the Scherrer formula [28]. The crystallite size appeared to increase upon increasing the MEEP molar ratio to Li-hectorite, which is possibly due to the significant enhancement in basal spacing upon loading of the polymer into the layered structure.
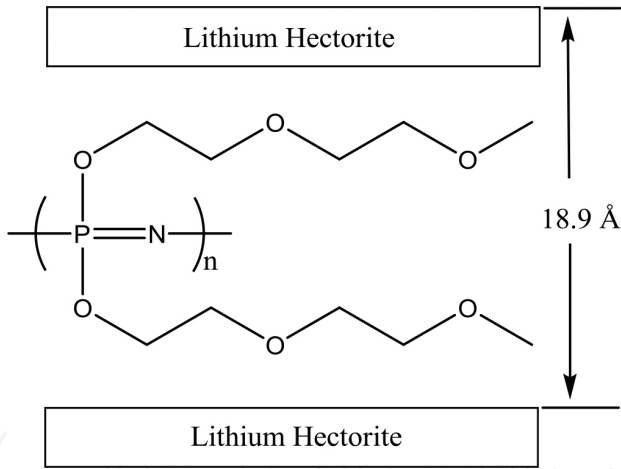


**Figure 4.** Schematic arrangement of MEEP in lithium hectorite (0.5:1).

The dimensions of MEEP were estimated using Spartan '08. The average dimension was determined for the largest possible distance between the ether oxygens on the R-groups in MEEP, and was found to be approximately 7.9 Å for one unit of MEEP [29]. This indicates that a single layer of MEEP is inserted between the Li-hectorite sheets for the MEEP:Li-hectorite (0.5:1) nanocomposite, which had a net layer expansion of 9.40 Å. The difference of 1.5 Å between the observed basal spacing of the 0.5:1 nanocomposite and the calculated dimensions of MEEP could be due to the manner in which MEEP is oriented within the layers. MEEP is a highly flexible polymer and may not necessarily be oriented within the layers as depicted in **Figure 4**. For example, a helical conformation may also be possible.

### 3.1.2. Thermogravimetric analysis

Thermogravimetric analysis was used to compare the thermal stability of MEEP, MEEP:Li-hectorite, Li-MEEP, and Li-MEEP:Li-hectorite. This was completed in order to monitor the thermal stability of nanocomposites with different polymer concentrations and to compare the stability of salt-complexed materials with their uncomplexed counterparts. The MEEP:Li-hectorite thermograms were also used to calculate the stoichiometry of the synthesized nanocomposites.

The thermogram of pristine MEEP (**Figure 5(c)**) shows that it undergoes a major decomposition between 230 and 350°C, followed by an onward gradual weight loss. Once MEEP is complexed with lithium triflate (LiCF$_3$SO$_3$), its decomposition is slightly compromised due to the presence of the inorganic salt, which appeared to decrease the polymer onset decomposition temperature by approximately 30°C; thereafter, complete decomposition of the triflate salt is observed at 420°C (**Figure 5(d)**).
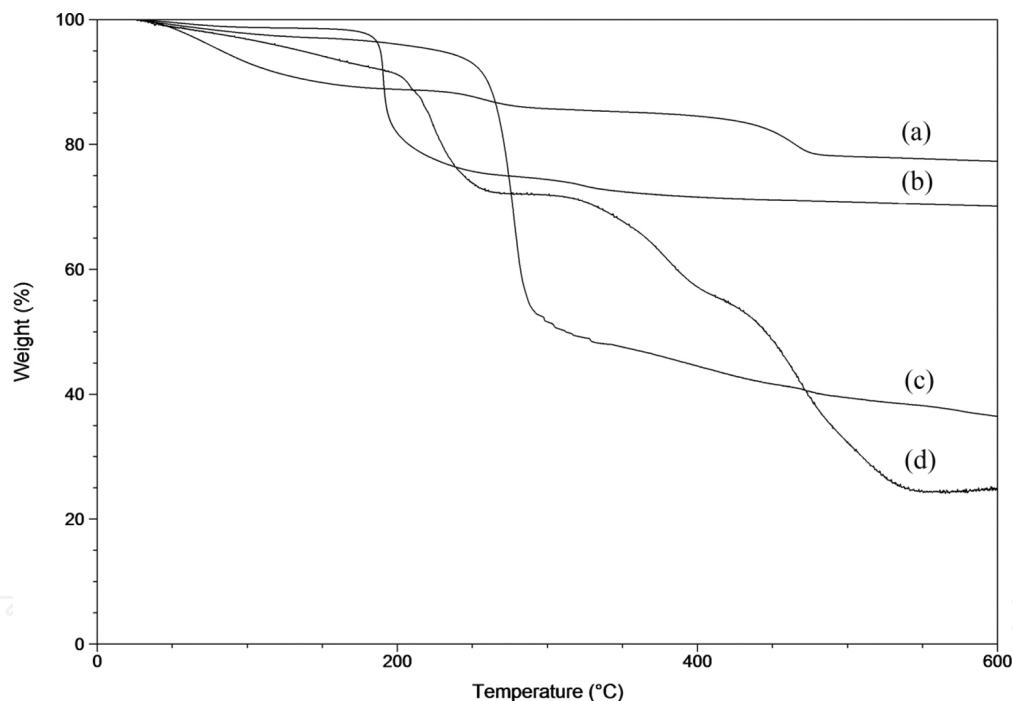


**Figure 5.** TGA data for (a) Li-MEEP:Li-hectorite (1:1), (b) MEEP:Li-hectorite(1:1), (c) MEEP, and (d) Li-MEEP.

Upon polymer intercalation, the nanocomposite thermograms appeared to have three weight loss steps, where the thermogram of, for example, MEEP:Li-hectorite (1:1) (**Figure 5(b)**) illustrates a small loss of water near 100°C, followed by the decomposition at 178°C corresponding to the presence of externally lying MEEP. The final decomposition is the gradual decomposition of the intercalated MEEP occurring at 305°C. This is quite similar to the thermal behavior of Li-MEEP:Li-hectorite (1:1) (**Figure 5(a)**), except for the decomposition of the salt which occurs at around 420°C. The TGA data are summarized in **Table 2**.

| Material | $T_a$ (°C) | $T_b$ (°C) | $\Delta T_c$ (°C) |
| --- | --- | --- | --- |
| MEEP | 240 | N/A | N/A |
| Li-MEEP | 204 | N/A | N/A |
| MEEP:Li-hectorite (0.5:1) | 205 | 312 | 72 |
| MEEP:Li-hectorite (1:1) | 178 | 305 | 65 |
| MEEP:Li-hectorite (2:1) | 176 | 315 | 75 |
| MEEP:Li-hectorite (4:1) | 170 | 324 | 84 |

$T_a$, onset decomposition temperature of pure MEEP or externally lying MEEP in nanocomposite; $T_b$, onset decomposition temperature of intercalated MEEP in nanocomposite; and $\Delta T_c$, difference in decomposition temperature of the intercalated MEEP and pristine MEEP.

**Table 2.** Thermogravimetric data.

As shown in **Table 2**, the onset decomposition temperatures of the externally lying MEEP ($T_a$) in the nanocomposites were lower than that of the bulk polymer, which occurs at 240°C. However, the onset decomposition temperatures of the intercalated MEEP ($T_b$) in the nano-composites are significantly higher than that of the pure polymer, indicating enhancement in the thermal stability of polymer when sandwiched between the layers of hectorite.

| MEEP:Li-hectorite (mol ratio) | Stoichiometry |
| --- | --- |
| 0.5:1 | $(H_2O)_{0.61}$ $(MEEP_{Ext})_{0.17}$ $(MEEP_{In})_{0.023}$(Li-hectorite) |
| 1:1 | $(H_2O)_{0.42}$ $(MEEP_{Ext})_{0.44}$ $(MEEP_{In})_{0.073}$(Li-hectorite) |
| 2:1 | $(H_2O)_{0.48}$ $(MEEP_{Ext})_{0.71}$$(MEEP_{In})_{0.12}$(Li-hectorite) |
| 4:1 | $(H_2O)_{0.34}$ $(MEEP_{Ext})_{0.84}$ $(MEEP_{In})_{0.14}$(Li-hectorite) |

**Table 3.** Stoichiometry of MEEP:Li-hectorite nanocomposites.

Since the nanocomposites displayed three decomposition steps, the stoichiometry was calculated in order to compare the spread between externally lying and intercalated polymer. It is important to note that the stoichiometry was calculated only for the MEEP:Li-hectorite nanocomposites, and not for the Li-MEEP:Li-hectorite nanocomposites due to the presence of lithium salt. The stoichiometry data of the nanocomposites are displayed in **Table 3**.

As shown in **Table 3**, when the molar ratio of MEEP is increased with respect to Li-hectorite, there is an increase in the amount of the externally lying polymer and intercalated polymer. These observations are in agreement with the XRD data (**Table 1**), which indicate that the basal spacing of the intercalated nanocomposite increases when the amount of MEEP is increased. In fact, MEEP:Li-hectorite (4:1) has almost twice as much of the intercalated polymer compared to MEEP:Li-hectorite (1:1).

### 3.1.3. Differential scanning calorimetry

Differential scanning calorimetry was used to monitor the glass transition temperature ($T_g$) of pristine MEEP, Li-MEEP, and their corresponding synthesized nanocomposites (**Figure 6**).
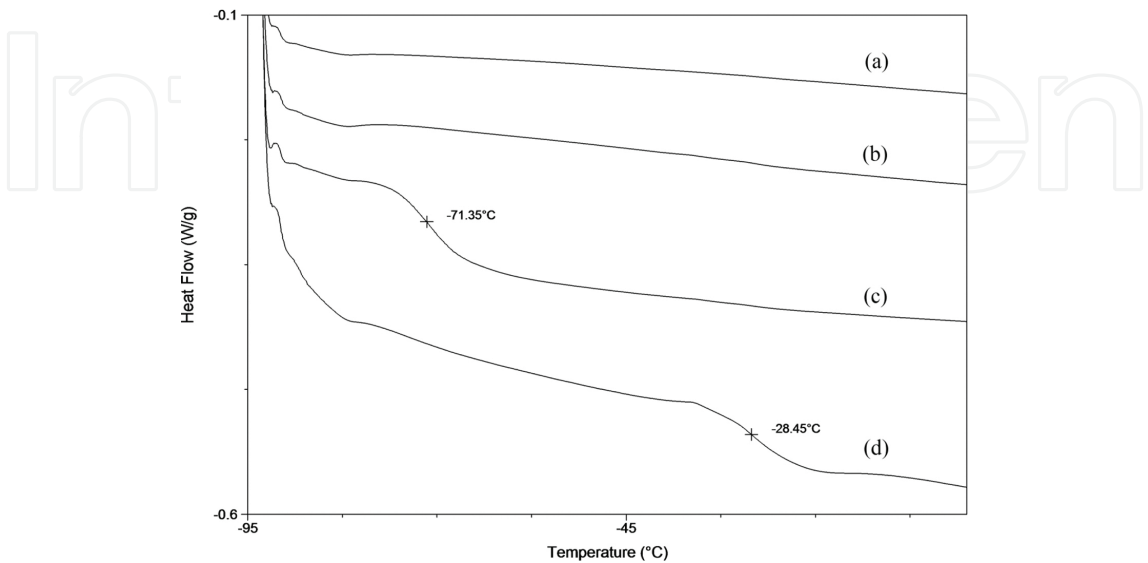


**Figure 6.** DSC data for (a) MEEP:Li-hectorite (1:1), (b) Li-MEEP:Li-hectorite (1:1), (c) MEEP, and (d) Li-MEEP.

| Material | ($T_g$, °C) |
|---|---|
| MEEP | −71 |
| Li-MEEP | −28 |
| MEEP:Li-hectorite (0.5:1) | − |
| MEEP:Li-hectorite (1:1) | − |
| MEEP:Li-hectorite (2:1) | − |
| MEEP:Li-hectorite (4:1) | − |

**Table 4.** Summary of DSC data.

The DSC of pure MEEP indicates a $T_g$ of −71°C, which is in fairly good agreement with the previously reported literature value of −83°C [30]. Upon complexing MEEP with lithium triflate (LiCF$_3$SO$_3$), the glass transition temperature ($T_g$) significantly increases to −28°C due to the crystalline nature of lithium triflate. However, upon intercalation of pristine MEEP or Li-MEEP into Li-hectorite, a $T_g$ is not observed for the ratios used. Due to the lack of glass transition temperatures in both Li-MEEP:Li-hectorite and MEEP:Li-hectorite nanocomposites, it is believed that (1) the oxygen atoms of the polymer are potentially interacting with the tetrahedrally coordinated silicon atoms in the hectorite sheets and restricting chain mobility or (2) the polymer is no longer flexible when it is intercalated in the layers of hectorite. The glass transition temperatures are displayed in **Table 4**.

### 3.1.4. Attenuated total reflectance

ATR spectroscopy was used to monitor the bond vibrations in MEEP, MEEP:Li-hectorite, Li-MEEP, and Li-MEEP:Li-hectorite. More specifically, it was important to determine whether intercalating MEEP or Li-MEEP into Li-hectorite hinders the flexibility of the polymer, and ultimately its ionic conductivity (**Figure 7**).
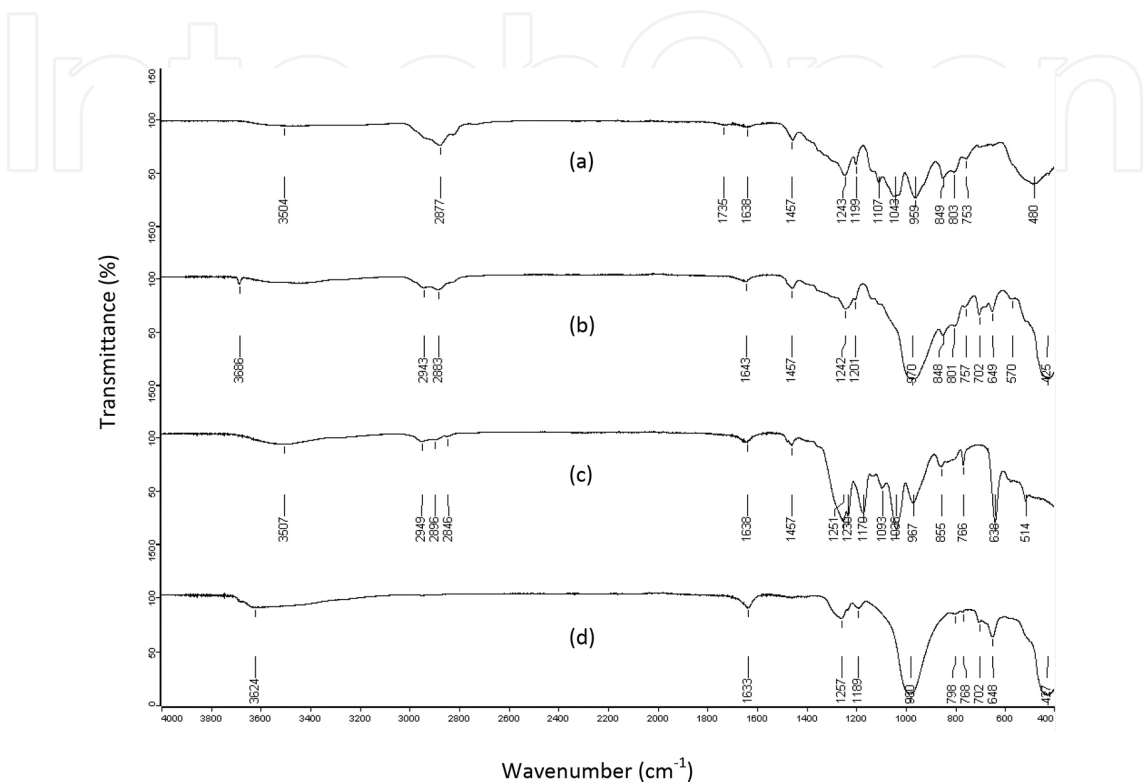


**Figure 7.** ATR results for (a) MEEP, (b) MEEP:Li-hectorite (1:1), (c) Li-MEEP, and (d) Li-MEEP:Li-hectorite(1:1).

| Major vibrations (cm⁻¹) | MEEP | MEEP:Li-hectorite(1:1) | Li-MEEP | Li-MEEP:Li-hectorite(1:1) |
|---|---|---|---|---|
| HOH stretch | N/A | 3686 | N/A | 3624 |
| Sp³ C-H stretch/bend | 2877/1457 | 2883/1457 | 2896/1457 | 2887/1457 |
| P=N | 1243 | 1242 | 1251 | 1257 |
| P-O-C | 959 | 967 | 980 | 972 |
| C-O-C ether | 1199–1043 | 1201 | 1170–1036 | 1189 |
| PNP skeletal | 849/803/753 | 848/801/757 | 855/766 | 798/768 |
| CF₃ | N/A | N/A | 1249 | 1253 |
| C-F deformation | N/A | N/A | 638 | 638 |
| SO₃ asymmetric bend | N/A | N/A | 573 | 573 |
| SO₃ symmetric bend | N/A | N/A | 518 | 518 |

**Table 5.** Summary of IR data.

From the IR data, it is observed that the P = N vibration in the pure polymer occurs at 1243 cm$^{-1}$. Upon complexation with lithium triflate, the P = N vibration of the polymer shifts to 1251 cm$^{-1}$, and to 1257 cm$^{-1}$ in the synthesized nanocomposites. This increase in vibrational energy of the P = N bond is indicative of the increased rigidity of the polymer backbone. The P-O-C vibration in MEEP shifts from 959 to 967 cm$^{-1}$ upon intercalation into Li-hectorite, indicating increased rigidity of the polymer side chains. Thus, the IR data support lack of polymer flexibility upon intercalation, and are in very good agreement with the DSC results. The IR data are summarized in **Table 5** [8].

### 3.1.5. AC impedance spectroscopy

Impedance measurements were conducted on Li-MEEP and the Li-MEEP:Li-hectorite nano-composites. Since the DSC and IR data indicated that the polymer-chain flexibility was restricted in the nanocomposites, it was necessary to investigate the ionic conductivity properties of Li-MEEP prior to intercalation, and post-intercalation. A complex plane plot of the impedance of an Li-MEEP sample is given in **Figure 8**. High-frequency data (10 kHz) is near the origin, and low-frequency (0.01 Hz) at the upper right.
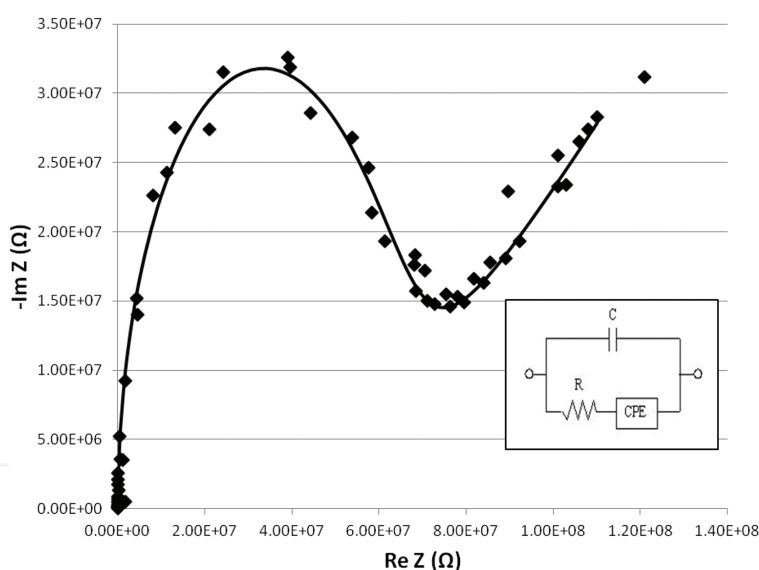


**Figure 8.** Complex-plane plot of Li-MEEP impedance at 300 K.

As shown in **Figure 8**, Li-MEEP demonstrates a curve typical for an ionic conductor. The value of Re(Z) at which Im(Z) goes through a minimum (about $7 \times 10^7$ Ω in **Figure 8**) corresponds approximately to the resistance (R) of the sample. The value of R and the dimensions of the polymeric film were used to calculate the ionic conductivity of the sample. In order to obtain more accurate values of R from the impedance data, a complex nonlinear least-squares fit was done with an equivalent circuit model using the program LEVMW [27]. A three-component equivalent circuit consisting of a resistor (R), a constant-phase element (CPE) that models the effects of the blocking electrodes, and a parallel capacitor (C) was used and is shown in the

inset of **Figure 8**. Using the resistance value $R$ and the dimensions of the polymeric film, the ionic conductivity of Li-MEEP was calculated.

Ionic conductivity measurements were performed within the temperature range of 220–310 K, and the results for a typical Li-MEEP sample are displayed in **Figure 9**. As is typical for ionically conducting polymers, the conductivity drops rapidly as the temperature is reduced, and for this sample it was too small to be measured with our system below 260 K.
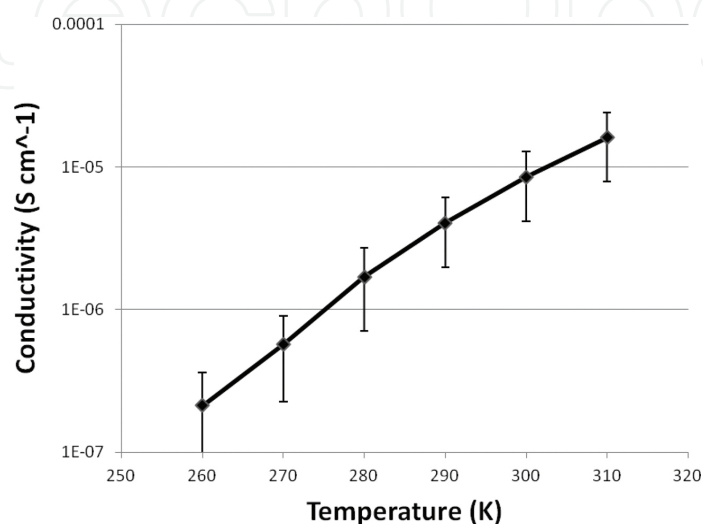


**Figure 9.** Variable-temperature ionic conductivity of Li-MEEP.

The room temperature ionic conductivity of Li-MEEP samples ranged from about $4 \times 10^{-6}$ to $1.3 \times 10^{-5}$ S/cm, which is in agreement with the literature [11, 12]. However, upon intercalation of Li-MEEP into Li-hectorite, the conductivity of the resulting nanocomposite material was below our detection limit, which in the case of these cast film samples is about $10^{-7}$ S/cm. These observations further indicate that there is an interaction occurring between the polymer and the layered structure that is ultimately inhibiting the nanocomposites from conducting lithium ions.

## 4. Conclusions

MEEP has been intercalated into Li-hectorite. A series of nanocomposites have been created by varying the mole ratio of the polymer with respect to the clay. The nanocomposites were characterized by TGA, DSC, FTIR, XRD, and AC impedance spectroscopy. XRD data confirm the successful and complete intercalation of MEEP into the layered silicate. TGA data confirm that increasing the molar ratio of MEEP with respect to the Li-hectorite results in a larger amount of the polymer within the layers. In fact, MEEP:Li-hectorite (4:1) has approximately twice the amount of intercalated polymer versus MEEP:Li-hectorite (1:1). TGA also indicates an enhancement in thermal stability of the intercalated polymer versus the pristine polymer for all nanocomposites. For instance, the intercalated polymer in MEEP:Li-hectorite (1:1) is

thermally stable up to 305°C, while the pure polymer decomposes at 240°C. The room temperature ionic conductivity of Li-MEEP was determined to be about $1 \times 10^{-5}$ S/cm; however, the polymer-salt complex displayed high ionic resistance when intercalated into Li-hectorite, and hence the ionic conductivity of the nanocomposites was too small to be determined (below about $10^{-7}$ S/cm). The impedance data are in good agreement with the DSC results, where no glass transition temperature has been detected for all the synthesized nanocomposites. ATR spectroscopy also confirms that the rigidity of the polymer backbone increases upon complexation with lithium triflate, and when the lithium complexed MEEP is intercalated into Li-hectorite.

## Acknowledgements

## Author details

Iskandar Saada[1], Rabin Bissessur[1*], Douglas C. Dahn[2] and Matthieu Hughes[2]

*Address all correspondence to: rabissessur@upei.ca

1 Chemistry Department, University of Prince Edward Island, Charlottetown, PE, Canada

2 Physics Department, University of Prince Edward Island, Charlottetown, PE, Canada

## References

[1] Johan MR, Shy OH, Ibrahim S, Yassin SSM, Hui TY. Effects of $Al_2O_3$ nanofiller and EC plasticizer on the ionic conductivity enhancement of solid PEO-LiCF$_3$SO$_3$ solid polymer electrolyte. Solid State Ionics. 2011;196:41–47. DOI:10.1016/j.ssi.2011.06.001

[2] Burjanadze M, Karatas Y, Kaskhedikar N, Kogel LM, Kloss S, Gentschev A-C, Hiller MM, Muller RA, Stolina R, Vettikuzha P, Weimhöfer H-D. Salt-in-polymer electrolytes for lithium ion batteries based on organo-functionalized polyphosphazenes and polysiloxanes. Z. Phys. Chem. 2010;224:1439–1473. DOI:10.1524/zpch.2010.0046

[3] Allcock HR, Kellam III EC. The synthesis and applications of novel aryloxy/oligoethyleneoxy substituted polyphosphazenes as solid polymer electrolytes. Solid State Ionics. 2003;156:401–414.

[4]   Allcock HR, Taylor JP. Phosphorylation of phosphazenes and its effects on thermal properties and fire retardant behaviour. Polymer Eng. Sci. 2010;40:1177–1189.

[5]   Fei S-T, Allcock HR. Methoxyethoxyethoxyphosphazenes as ionic conductive fire retardant additives for lithium battery systems. J. Power Sources. 2010;195:2082–2088. DOI:10.1016/j.jpowsour.2009.09.043

[6]   Fei S-T, Lee S-HA, Pursel SM, Basham J, Hess A, Grimes CA, Horn MW, Mallouk TE, Allcock HR. Electrolyte infiltration in phosphazene-based dye-sensitized solar cells. J. Power Sources. 2011;196:5223–5230.

[7]   Allcock HR, O'Connor SJM, Olmeijer DL, Napierala ME, Cameron CG. Polyphosphazenes bearing branched and linear oligoethyleneoxy side groups as solid solvents for ionic conduction. Macromolecules. 1996;29:7544–7552.

[8]   Nazri G, MacArthur DM, Ogara JF. Polyphosphazene electrolytes for lithium batteries. Chem. Mater. 1989;1:370–374. DOI:10.1021/cm00003a019

[9]   Abraham KM, Alamgir M. Dimensionally stable MEEP-based polymer electrolytes and solid-state lithium batteries. Chem. Mater. 1991;3:339–348. DOI:10.1021/cm00014a027

[10]  Scully SF, Bissessur R, MacLean KW, Dahn DC. Inclusion of poly[bis(methoxyethoxyethoxy)phosphazene] into layered graphite oxide. Solid State Ionics. 2009;180:216–221.

[11]  Blonsky PM, Shriver DF, Austin P, Allcock HR. Polyphosphazene solid electrolytes. J. Am. Chem. Soc. 1984;106:6854–6855. DOI:10.1021/ja00334a071

[12]  Silva VPR, Silva GG, Caliman V, Rieumont J, de Miranda-Pinto COB, Archanjo BS, Neves BRA. Morphology, crystalline structure and thermal properties of PEO/MEEP blends. Eur. Polymer J. 2007;43:3283–3291.

[13]  Allcock HR, Chang Y, Welna DT. Ionic conductivity of covalently interconnected polyphosphazene–silicate hybrid networks. Solid State Ionics. 2006;177:569–572. DOI: 10.1016/j.ssi.2005.11.017

[14]  Bissessur R, Gallant D, Brüning R. New poly[bis-(methoxyethoxyethoxy)phosphazene]–$MoS_2$ nanocomposite. Solid State Ionics. 2003;158:205–209. DOI:10.1016/S0167-2738(02)00774-9

[15]  Hutchison JC, Bissessur R, Shriver DF. Enhancement of ion mobility in aluminosilicate-polyphosphazene nanocomposites. Mat. Res. Soc. Symp. Proc. 1996;457:489–494.

[16]  Scully SF, Bissessur R. Encapsulation of polymer electrolytes into hectorite. Appl. Clay. Sci. 2010;47:444–447. DOI:10.1016/j.clay.2009.12.023

[17]  Madejová J, Bujdák J, Janek M, Komadel P. Comparative FT-IR study of structural modifications during acid treatment of dioctahedral smectites and hectorite. Spectrochim. Acta. Part A. 1998;54:1397–1406.

[18]  Carretero MI, Pozo M. Clay and non-clay minerals in the pharmaceutical industry Part I. Excipients and medical applications. Appl. Clay Sci. 2009;46:73–80. DOI:10.1016/j.clay.2009.07.017

[19]  Okada A, Usuki A. The chemistry of polymer-clay hybrids. Mater. Sci. Eng. C. 1995;3:109–115.

[20]  Sandí G, Carrado KA, Joachin H, Lu W, Prakash J. Polymer nanocomposites for lithium battery applications. J. Power Sources. 2003;119–121:492–496. DOI:10.1016/S0378-7753(03)00272-6

[21]  Riley M, Fedkiw PS, Khan SA. Transport properties of lithium hectorite-based composite electrolytes. J. Electrom. Soc. 2002;149:A667–A674. DOI:10.1149/1.1470652

[22]  Carrado KA, Forman JE, Botto RE, Winans RE. Incorporation of phthalocyanines by cationic and anionic clays via ion exchange and direct synthesis. Chem. Mater. 1993;5:472–478.

[23]  Singhal RG, Capracotta MD, Martin JD, Khan SA, Fedkiw PS. Transport properties of hectorite based nanocomposite single ion conductors. J. Power Sources. 2004;128:247–255.

[24]  Allcock HR, Austin PE, Neenan TX, Sisko JT, Blonsky PM, Shriver DF. Polyphosphazenes with etheric side groups: prospective biomedical and solid electrolyte polymers. Macromolecules. 1986;19:1508–1512.

[25]  Blonsky PM, Shriver DF, Austin P, Allcock HR. Complex formation and ionic conductivity of polyphosphazene solid electrolytes. Solid State Ionics. 1986;18–19:258–264.

[26]  Barsoukov E, Macdondald JR, editors. Impedance Spectroscopy Theory, Experiments, and Applications, 2nd ed. Hoboken, New Jersey, Wiley; 2005.

[27]  Macdonald JR. 2015. Available at: jrossmacdonald.com/levmlevmw [accessed 25 June 2015].

[28]  Monshi A, Foroughi MR, Monshi MR. Modified Scherrer equation to estimate more accurately nano-crystalline size using XRD. World J. Nano Sci. Eng. 2012;2:154–160.

[29]  Spartan '08. Wavefunction Inc., Irvine, CA; 2008.

[30]  Allcock HR, Napierala ME, Olmeijer DL, Cameron CG, Kuharcik SE, Reed CS, O'Connor SJM. New macromolecules for solid polymeric electrolytes. Electrochim. Acta. 1998;43:1145–1150.